A Dimensionless Model for Predicting the Mass-Transfer Area of Structured Packing

Robert E. Tsai, A. Frank Seibert, R. Bruce Eldridge, and Gary T. Rochelle
Dept. of Chemical Engineering, Process Science and Technology Center, The University of Texas at Austin, Austin, TX 78712

DOI 10.1002/aic.12345
Published online August 30, 2010 in Wiley Online Library (wileyonlinelibrary.com).

The mass-transfer area of nine structured packings was measured in a 0.427 m ID column via absorption of CO_2 from air into 0.1 kmol/m^3 NaOH. The mass-transfer area was most strongly related to the specific area (125–500 m^2/m^3), and liquid load (2.5–75 $m^3/m^2 \cdot h$). Surface tension (30–72 mN/m) had a weaker but significant effect. Gas velocity (0.6–2.3 m/s), liquid viscosity (1–15 mPa·s), and flow channel configuration had essentially no impact on the mass-transfer area. Surface texture (embossing) increased the effective area by 10% at most. The ratio of mass-transfer area to specific area (a_e/a_p) was correlated within the limits of ±13% for the entire experimental database $\frac{a_e}{a_p} = 1.34\left[\left(\frac{\rho_L}{\sigma}\right) g^{1/3}\left(\frac{Q}{L_p}\right)^{4/3}\right]^{0.116}$. © 2010 American Institute of Chemical Engineers

AIChE J, 57: 1173–1184, 2011
Keywords: absorption, mass transfer, structured packing, effective area

Introduction

Packing is commonly used in absorption and distillation columns to promote efficient gas-liquid contacting. Packing performance can be assessed in terms of mass-transfer coefficients (k_G or k_L^0) and the effective mass-transfer area (a_e). For CO_2 capture by aqueous amine absorption, structured packing is an attractive option because of its favorable mass transfer and hydraulic characteristics.[1,2] Under most conditions, the CO_2-amine reaction is fast enough such that the CO_2 reacts within a short distance of the gas-liquid interface. Consequently, the only packing-related mass-transfer parameter that the CO_2 flux depends on in this application is the effective area. Therefore, a reliable structured packing area model is especially critical for the analysis and design of these processes.

Wang et al.[3] performed an extensive review of the numerous structured packing area correlations that have been proposed and noted that the problem has not been satisfactorily solved. Various issues with the models are apparent. Many rely on packing-specific constants, which limit their adaptability and also imply a degree of discontinuity between the seemingly relatable packings. The different correlations predict contrasting effects of properties like liquid viscosity and surface tension as well, indicating that the internal fluid flow behavior is not well understood. It is evident that there is ample margin for improvement in current predictive capabilities.

The mass-transfer correlations of Rocha et al.[4] and Billet and Schultes[5] are two widely used models for structured packing. Both drew on extensive experimental databases involving a variety of fluid systems and, therefore, in theory, captured a range of physical properties and their associated effects. The models were validated with overall mass transfer data (e.g., *HETP*). The individual parameters (e.g., a_e), however, were basically forced to fit these results and were not independently verified.

Consequently, it is possible that the correlations have been inherently confounded by interacting effects. For instance, a viscosity impact on mass transfer may have been correlated with the effective area, when it really should have been associated with the mass-transfer coefficient. This disconnect

Correspondence concerning this article should be addressed to R. E. Tsai at tsai@che.utexas.edu.

makes it difficult to use these correlations with a high level of confidence.

Characterization methods exist that allow for the decoupling of the mass-transfer parameters via appropriate test system selections and, thereby, facilitate a cleaner interpretation of the mass-transfer performance.[6,7] This work was in consensus with this approach, with the specific objective being the development of an improved mass-transfer area model for structured packing. The basis of this *area* model was a comprehensive set of *area* data; effective areas of a variety of packings were evaluated as a function of liquid load, liquid viscosity, and surface tension. The experiments were planned with the physical property ranges of amine solvents in mind,[8–12] although the test conditions were certainly of general relevance as well. Measurements were made via the absorption of dilute CO_2 into aqueous NaOH. This method has been identified by Sharma and Danckwerts,[13] among many others, as a convenient means by which gas-liquid interfacial areas can be determined. With sufficient free hydroxide, the concentration of bicarbonate (HCO_3^-) is negligible, and the overall reaction may be written as

$$CO_2(aq) + 2OH^- \rightarrow CO_3^{2-} + H_2O \quad (1)$$

The reaction can be considered as practically irreversible, with a rate expression given by Eq. 2

$$r = k_{OH^-}[OH^-][CO_2] \quad (2)$$

When CO_2 partial pressures are low and hydroxide ion is present in relative excess, the reaction can be treated as pseudo-first-order. Equation 2 consequently simplifies to

$$r \cong k_1[CO_2] \quad (3)$$

Experimental

Materials

The NaOH solutions for wetted-wall column experiments were purchased from Fisher Scientific (certified grade). The solutions for packed column tests were prepared using solid NaOH pellets (PHARMCO-AAPER, 98.5% or EMD Chemicals, Inc., 97.0%). The difference in solution preparation was a matter of convenience and was not believed to adversely affect the comparability of the experiments. A nonionic surfactant, TERGITOL™ NP-7 (Dow), was used to reduce the surface tension of solutions. POLYOX™ WSR N750 (Dow) — essentially, poly(ethylene oxide) with a molecular weight of 300,000 — was employed as a viscosity enhancer. With both of these reagents, suppression of foam was found to be necessary, particularly during packed column experiments. Dow Corning® Q2-3183A antifoam was used for this purpose in concentrations typically ranging from 50–100 g/m^3.

Packed column

The packed column had an outside diameter of 0.46 m, an inside diameter of 0.427 m, and a 3-m packed height. Operation was countercurrent, with ambient air entering below the packed bed and flowing upward through the tower. The liquid (typically 0.75 m^3 inventory) was pumped in a closed loop and was distributed at the top of the column using a pressurized fractal distributor with 108 drip points/m^2. This density was believed to be sufficient to avoid maldistribution and other undesirable effects, based on past distributor studies conducted by the Separations Research Program (SRP) at the University of Texas at Austin. In the literature, Perry et al.[14] also reported a distribution density of 100 points/m^2 to be satisfactory for most packings. Additional details about the experimental system are in Tsai et al.[15] and a complete procedural description can be found in Tsai.[16]

Wetted-wall column (WWC)

The wetted-wall column (WWC) was a bench-scale gas-liquid contactor with a known interfacial area (38.52 cm^2) that was used to measure the kinetics of various systems. The apparatus has previously been used and described by Bishnoi and Rochelle,[17] Cullinane and Rochelle,[18] and Tsai et al.[15]

Supplementary equipment

The goniometer (ramé-hart, Inc., model #100-00) included an adjustable stage, a syringe support arm, a computer-linked camera for live image display, and a light source. This system was used with FTA32 Video 2.0 software (developed by First Ten Angstroms, Inc.) to make surface tension measurements via pendant drop analysis.

A Physica MCR 300 rheometer (Anton Paar, USA) equipped with a cone-plate spindle (CP 50-1) was used for viscosity measurements. Temperature was regulated ($\pm$0.1°C) with a Peltier unit (TEK 150P-C) and a Julabo F25 water bath unit (for counter-cooling). Measurement profiles consisted of a logarithmically ramped or decremented shear rate (100–500 s^{-1}), with a minimum of 10 points taken at 15 s intervals.

Governing equations and data analysis

A gas and liquid film can be envisioned to be in contact for the case of gas absorption into a liquid, and the flux can be written in terms of an overall mass-transfer coefficient (K_G), gas-side mass-transfer coefficient (k_G), or liquid-side mass-transfer coefficient (k_L^0). In scenarios involving absorption with chemical reaction, a term known as the enhancement factor (E) is commonly encountered. It reflects the increase in mass transfer due to the reaction relative to physical diffusion. In this situation, the flux of gas (CO_2) on the basis of the liquid-side mass-transfer coefficient is given by Eq. 4

$$N_{CO_2} = Ek_L^0\left([CO_2]^i - [CO_2]\right) = \frac{Ek_L^0}{H_{CO_2}}\left(P_{CO_2}^i - P_{CO_2}^*\right) \quad (4)$$

In Eq. 4, the CO_2 partial pressure and concentration have been related by a distribution coefficient (H_{CO2}), and the superscripts i and *, respectively, denote the interface and equilibrium partial pressures (or concentrations). The parameters in this equation can be grouped into a single term for convenience, hence, defined as k_g'

$$k'_g = \frac{Ek^0_L}{H_{CO_2}} \tag{5}$$

For the case of diffusion-controlled absorption with a fast, irreversible reaction under the assumption of pseudo-first-order conditions, an expression for the CO_2 flux can be obtained via solution of any of the various mass-transfer theories (i.e., film theory, penetration theory, etc.).[19] The solution using surface renewal theory has been presented in the literature[17,20] and has been selected for display here, starting from Eq. 6

$$N_{CO_2} = k^0_L \sqrt{1 + \frac{k_1 D_{CO_2,L}}{(k^0_L)^2}} \frac{\left(P^i_{CO_2} - P^*_{CO_2}\right)}{H_{CO_2}} \tag{6}$$

Equation 6 is notably relatable to Eq. 4 via the enhancement factor

$$E = \sqrt{1 + \frac{k_1 D_{CO_2,L}}{(k^0_L)^2}} \tag{7}$$

The Hatta number (Ha) for pseudo-first-order reactions has been defined in various sources[21,22]

$$Ha = \frac{\sqrt{k_1 D_{CO_2,L}}}{k^0_L} \tag{8}$$

For $Ha^2 \gg 1$, as was the case for the experiments that were conducted, the Hatta number and enhancement factor are approximately equal, and Eq. 6 can be simplified to

$$N_{CO_2} \cong \frac{\sqrt{k_1 D_{CO_2,L}}}{H_{CO_2}} \left(P^i_{CO_2} - P^*_{CO_2}\right) \tag{9}$$

Combination of Eqs. 4, 5, and 9 leads to the following theoretical expression for k'_g

$$k'_g = \frac{\sqrt{k_1 D_{CO_2,L}}}{H_{CO_2}} = \frac{\sqrt{k_{OH^-}[OH^-] D_{CO_2,L}}}{H_{CO_2}} \tag{10}$$

The performance of both the WWC and the packed column was modeled by series resistance (Eq. 11)

$$\frac{1}{K_G} = \frac{1}{k_G} + \frac{H_{CO_2}}{Ek^0_L} = \frac{1}{k_G} + \frac{1}{k'_g} \tag{11}$$

For the WWC experiments, the overall mass-transfer coefficient (K_G) was determined from the CO_2 flux and the partial pressure driving force. The gas-side mass-transfer coefficient (k_G) was a function of physical properties, and was calculated using a WWC-specific correlation.[17] Equation 11 was then solved for k'_g. These experimental values were compared with calculated ones (Eq. 10), evaluated using the correlations of Pohorecki and Moniuk[23] for the diffusion coefficient ($D_{CO_2,L}$), Henry's constant (H_{CO_2}), and reaction rate constant (k_{OH-}).

The differential mass balance associated with absorption in a packed column is given by Eq. 12

$$u_G \frac{dy}{dz} = (K_G a_e)(RT)(y^* - y) \tag{12}$$

The packed column experimental system was regarded as dilute, and a CO_2 equilibrium partial pressure of zero was assumed. The vapor flow rate (u_G) and volumetric mass-transfer coefficient ($K_G a_e$) were considered to be constant. Under these conditions, integration of Eq. 12 over the packed bed height (Z) yields the following expression for the volumetric mass-transfer coefficient

$$K_G a_e = \frac{u_G}{ZRT} \ln\left(\frac{y_{CO_2,in}}{y_{CO_2,out}}\right) \tag{13}$$

Gas-side resistance was intentionally limited by using dilute caustic solution (0.1 kmol/m^3), and operating at high-superficial air velocities — typically 0.6, 1, or 1.5 m/s, although one run at 2.3 m/s was also conducted as a check on gas-side resistance. This resistance was calculated from the correlation of Rocha et al.[4] to account for 1–2% of the overall mass-transfer resistance on average; measurements consisting of the absorption of SO_2 into caustic solution have supported this estimate. The $1/k_G$ term in Eq. 11 was neglected, and K_G was assumed to be equal to k'_g. The effective area (a_e) could subsequently be separated out from Eq. 13 by dividing through by k'_g.

$$a_e = \frac{u_G \ln\left(\frac{y_{CO_2,in}}{y_{CO_2,out}}\right)}{ZK_G RT} \approx \frac{u_G \ln\left(\frac{y_{CO_2,in}}{y_{CO_2,out}}\right)}{Zk'_g RT} = \frac{u_G \ln\left(\frac{y_{CO_2,in}}{y_{CO_2,out}}\right)}{ZRT} \times \frac{H_{CO_2}}{\sqrt{k_{OH^-}[OH^-] D_{CO_2,L}}} \tag{14}$$

To legitimately interpret k'_g in the manner outlined previously (Eq. 10), Ha^2 must be large, and there must be minimal interfacial depletion of reactants. Haubrock et al.[22] among others, quantified these requirements:

1. $Ha > 2$
2. $E_\infty/Ha > 5$

The enhancement factor for an instantaneous, irreversible reaction (E_∞) is defined in Eq. 15

$$E_\infty = 1 + \frac{D_{OH^-,L}[OH^-] H_{CO_2}}{D_{CO_2,L} P^i_{CO_2}} \tag{15}$$

All of the experiments performed in this work satisfied these conditions. For reference, Ha^2 for the WWC was on the order of 10^2. k^0_L was estimated from the theories of Pigford,[24] Hobler,[25] and Bird et al.,[26] which Pacheco[27] found to match experimentally measured values within 15%. The large Ha^2 criterion was slightly weaker for the packed column tests. Ha^2 was 12 in the absolute worst case, but it was at least 30 for 95% of the recorded data points. Here, k^0_L was calculated from the correlation of Rocha et al.[4]

Table 1. Summary of WWC Results (Experimental Conditions: 27–35°C, 0.11–0.32 m/s (Gas), 1.5–4.2 cm^3/s (Liquid), 150–630 Pa CO_2 at Inlet)

Test system	Approx. μ_L and/or σ	Number of data points	Normalized k_g'
0.1 $kmol/m^3$ NaOH (Baseline)	0.8 mPa·s, 70 mN/m	111	1.10 ± 0.09
0.1 $kmol/m^3$ NaOH + 125 ppm_v TERGITOL NP-7 + 50 g/m^3 Dow Corning Q2-3183A antifoam	30 mN/m	32	1.09 ± 0.07
0.1 $kmol/m^3$ NaOH + 1.25 wt % POLYOX WSR N750	8 mPa·s	10	0.94 ± 0.05

The aforementioned analysis assumes average values of the mass-transfer coefficients (k_G and k_L^0). In reality, we might expect lower values in stagnant regions and greater values in turbulent regions. It is improbable that a distribution of gas-side mass-transfer coefficients would have any appreciable effect on the measured area; however, since the gas-side resistance ($1/k_G$) was so much smaller (ca. two-orders of magnitude) than the liquid-side resistance ($1/k_g'$). A smaller liquid-side mass-transfer coefficient would result in greater interfacial depletion of hydroxide, but this issue is insignificant because the average E_∞/Ha is 500 to 1,000. The operating region approached the physical absorption regime in some instances (Ha ranged from about 5 to 25), so the interpretation of the area measurements could be affected by greater local values of the liquid-side mass-transfer coefficient.

Wetted-Wall Column (WWC) Results

The WWC was used to evaluate the baseline CO_2-NaOH k_g' values. It was also used to test for potential impacts of the property-modifying additives (TERGITOL NP-7 or POLYOX WSR N750) on k_g'. The WWC results are summarized in Table 1, expressed as a normalized k_g' (experimental k_g'/calculated k_g'). For the base case and surfactant systems, the calculated k_g' was simply the "Pohorecki" k_g'. For the POLYOX system, a different $D_{CO2,L}$ was applied to account for the polymer-based viscosity enhancement, in accordance with the work of Lohse et al.[28] This rather interesting modification was discussed in detail in Tsai et al.[29]

The baseline measurements gave values of k_g' that were 10% higher than predicted by Pohorecki and Moniuk.[23] One could argue based on these results that the Pohorecki k_g' was in need of a small corrective factor. Nevertheless, the disparity was not believed to be sufficient to dismiss the model, given the deviation in the WWC points (also around 10%) and the fact that the model seemed to adequately match the variation with temperature observed in the data (see Tsai[16]). The Pohorecki k_g' was presumed to be acceptable for the interpretation of the packing area measurements (Eq. 14). There was no statistically confirmable impact of surfactant and antifoam, implying that the same k_g' could be applied in this case as well; explanations for this result were offered in Tsai et al.[15] The WWC data with POLYOX WSR N750 were in good agreement with the Lohse-corrected Pohorecki k_g' values; this combined k_g' model was consequently used for packing experiments involving this system.

Misinterpretation of the WWC data was certainly an acknowledgeable concern, since the calculated packing area is directly dictated by k_g' (Eq. 14). If the Pohorecki model was indeed underpredictive by 10%, as suggested by the WWC data, then the areas reported in this research would be off by 10%. A similar conjecture can be made with respect to the POLYOX system and the subsequently interpreted impact of viscosity on the effective area. While this potential for error cannot be outright dismissed from the discussion to follow, it should be reiterated that the normalized k_g' results were near unity for all three investigated systems, indicating that the data and models were at least relatively consistent. The k_g' values that were applied in the analysis of the packing area measurements were believed to be accurate.

Packing Mass-Transfer Area Results

Global model

Table 2 lists the packings included in the mass transfer area database, along with their relevant dimensions and approximate conditions at which they were tested. The low-surface tension (30 mN/m), and high-viscosity (ca. 10 mPa·s) conditions were simulated using the same additives as tested in the WWC — that is, 125 ppm_v TERGITOL NP-7 and 1.25 wt % POLYOX WSR N750, respectively. Moderate viscosity (ca. 5 mPa·s) cases were run using a lower concentration of POLYOX WSR N750 (0.85 wt %). This midpoint was not explicitly investigated in the WWC, since its characterization was not critical. The results would presumably be encompassed within those of the high-viscosity scenario (1.25 wt % POLYOX WSR N750), where only minor effects were observed. Antifoam concentration sometimes varied (50–100 g/m^3) compared to the specific WWC experiments, but this was not believed to affect the k_g' interpretation. The channel dimensions (Figure 1) were defined in the same fashion as in other publications.[30,31] All of the packings were stainless steel and were manufactured by Sulzer Chemtech (Mellapak™ and MellapakPlus™), with the exception of Flexipac™ 1Y (Koch-Glitsch, Inc.) and the prototype 500-series packing. Every packing surface was perforated.

Dimensionless numbers were used to correlate the database. The effective area for structured packing is anticipated to primarily be attributable to liquid in contact with the packing surface, so the characteristic length was logically defined by a liquid film thickness. The resemblance of the flow channels to simple inclined plates suggested that it might be appropriate to apply the "classical" Nusselt film thickness (e.g., as defined in Bird et al.[26]) in the calculation of this parameter (Eq. 16)

$$\delta = \sqrt{\frac{3u_{L,film}\mu_L}{\rho_L g \sin\alpha}} = \sqrt[3]{\frac{3\mu_L}{\rho_L g \sin\alpha}\left(\frac{Q}{L_p}\right)} \qquad (16)$$

Table 2. Packings and Experimental Conditions Included in Mass Transfer Area Database

Packing	Specific area, a_p (m^2/m^3)	Corrugation angle, α (°)	Channel side, S (mm)	Channel base, B (mm)	Crimp height, h (mm)	Parameter source(s)	Conditions: μ_L[a] (mPa·s)/σ[b] (mN/m)
Mellapak 250Y (M250Y)	250	45	17	24.1	11.9	Petre et al.[32]	1/73, 0.8/31, 4/58, 14/44
Mellapak 500Y (M500Y)	500	45	8.1	9.6	6.53	Aroonwilas[33]	1/73, 0.9/31, 4/45, 10/42
Mellapak 250X (M250X)	250	60	17	24.1	11.9	Suess and Spiegel[34] Measured	1/73, 1/30, 11/42
MellapakPlus 252Y (MP252Y)	250	45	17	24.1	11.9	Alix and Raynal[35] Measured	0.8/71, 0.8/30, 8/42
Mellapak 250Y (smooth) (M250YS)	250[c]	45	17	24.1	11.9	Measured	1.1/73, 1/31
Mellapak 125Y (M125Y)	125	45	37	55	24.8	Spiegel and Meier[36] Measured	0.9/72, 0.8/31
Mellapak 2Y (M2Y)	205	45	21.5	33	13.8	Sulzer Chemtech Measured	0.9/72
Flexipac 1Y (F1Y)	410	45	9	12.7	6.4	Koch-Glitsch Petre et al.[32]	0.8/71, 6/63
Prototype 500 (P500)	500	45	8.1	9.6	6.53	Assumed same as M500Y	0.9/72, 0.9/31

[a]For base case system (0.1 kmol/m^3 NaOH), calculated from correlation of Moniuk and Pohorecki.[37]
[b]For base case system (0.1 kmol/m^3 NaOH), assumed same as water and calculated from fit of data in Haar et al.[38]
[c]Denotes uncertainty in actual specific area.

The best fit of the database (based on R^2 values) was obtained from a regression in the form of Eq. 17. The constants and standard errors are shown in Eq. 17a. (The M250YS data were not included in this regression due to uncertainty regarding the specific area of this packing, as will be explained later.)

$$\ln\left(\frac{a_e}{a_p}\right) = \ln a_f = C_1 \ln(We_L) + C_2 \ln(Fr_L) + C_3 \tag{17}$$

$$\ln a_f \pm 0.065; \quad C_1 = 0.112 \pm 0.003; \quad C_2 = -0.032 \pm 0.004; \quad C_3 = 0.271 \pm 0.014 \tag{17a}$$

The Weber and Froude numbers, subject to the appropriate substitutions, are shown in Eqs. 18 and 19

$$We_L = \frac{\rho_L u_{L,film}^2 \delta}{\sigma} = \frac{1}{\sigma}\left[\frac{\rho_L^4 g\,(\sin\alpha)}{3\mu_L}\left(\frac{Q}{L_p}\right)^5\right]^{1/3} \tag{18}$$

$$Fr_L = \frac{u_{L,film}^2}{g\delta} = \frac{\rho_L \sin\alpha}{3\mu_L}\left(\frac{Q}{L_p}\right) \tag{19}$$

The Froude number coefficient (C_2) was noticed to be roughly one-third of the Weber number coefficient (C_1) in Eq. 17. (The ratio is admittedly not quite one-third based on the numbers in Eq. 17a, but it was nearly exact when the analysis was initially performed, with a smaller database.) This correspondence was thought to possibly be significant, so a follow-up regression was performed where the Weber and Froude numbers were fixed in this ratio (Eq. 20)

$$\ln a_f = C_1 \ln\left[(We_L)(Fr_L)^{-1/3}\right] + C_2 \tag{20}$$

$$\ln a_f \pm 0.065; \quad C_1 = 0.116 \pm 0.002; \quad C_2 = 0.292 \pm 0.009 \tag{20a}$$

The final form of the area model, obtained upon rearrangement of Eq. 20, is displayed in Eq. 21

$$a_f = 1.34\left[(We_L)(Fr_L)^{-1/3}\right]^{0.116} \tag{21}$$

The $(We_L)Fr_L^{-1/3.}$ grouping is shown expanded in Eq. 22, with the wetted perimeter (L_p) specified in terms of the packing geometry (Eq. 23)

$$(We_L)(Fr_L)^{-1/3} = \left(\frac{\rho_L}{\sigma}\right) g^{1/3}\left(\frac{Q}{L_p}\right)^{4/3} = \left(\frac{\rho_L}{\sigma}\right) g^{1/3}\left(\frac{Q}{A}\cdot\frac{Bh}{4S}\right)^{4/3} \tag{22}$$

$$L_p = \frac{4S}{Bh}A \tag{23}$$

It should be noted that for this system (air–water), a correction to the gravitational constant (g) due to factors like

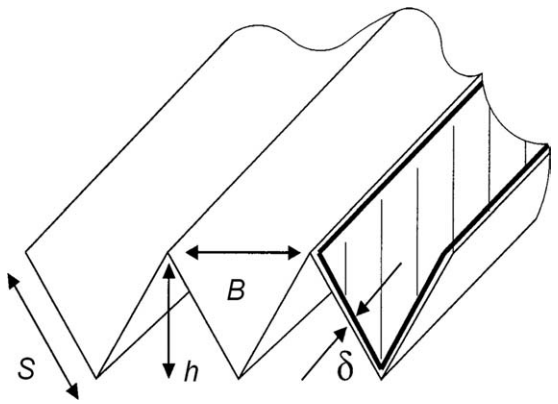

Figure 1. Packing channel dimensions.
Slightly modified version of image from Olujic et al.[30]

gas density was not believed to be necessary, but the incorporation of an "effective gravity" term, such as that proposed by Rocha et al.[39] could warrant consideration if applying Eq. 21 to other applications — for example, those at high-pressure.

Figure 2 is a plot of the entire packing mass-transfer area database, along with Eq. 21 and dashed lines denoting two standard deviations (±13%). The data can be found in detailed, tabulated form in Tsai.[16] The fit of the model was quite acceptable given the broad scope of the database, which as indicated in Table 2, consisted of packing sizes ranging from 125–500 m^2/m^3, viscosity from roughly 1–15 mPa·s, and surface tension from 30–72 mN/m. The liquid load and specific area, reflected in the flow rate per wetted perimeter term (Q/L_p) in Eq. 22, most strongly dictated the mass-transfer area. Surface tension and liquid density were also correlated as relevant parameters, although the latter was never explicitly varied. Gas velocity and liquid viscosity were notably absent from the model; both were concluded to have a negligible effect on area over the range of values tested. Also not included were terms involving the packing corrugation angle (M250X), element interface (MP252Y), and surface texture (M250YS), since none of these geometric features were found to appreciably affect the effective area. These results are all discussed in detail in the subsequent sections.

Effect of liquid load and packing size (M125Y/M250Y/F1Y/M500Y)

Figure 3 illustrates the strong influence of both liquid load (2.5–75 $m^3/m^2{\cdot}h$), and packing size (125–500 m^2/m^3) on the mass-transfer area. Every packing exhibited an increase in area with increasing liquid load, which was naturally attributable to a greater portion of the packing being wetted and, therefore, available to participate in the mass-transfer process.

The standard M250Y packing performed well on a fractional area basis. Its specific area was clearly being well

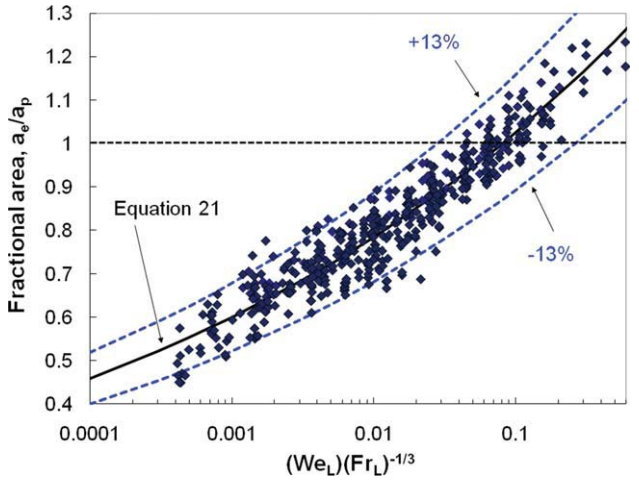

Figure 2. Structured packing mass-transfer area database, compared with global correlation (Eq. 21).

[Color figure can be viewed in the online issue, which is available at wileyonlinelibrary.com.]

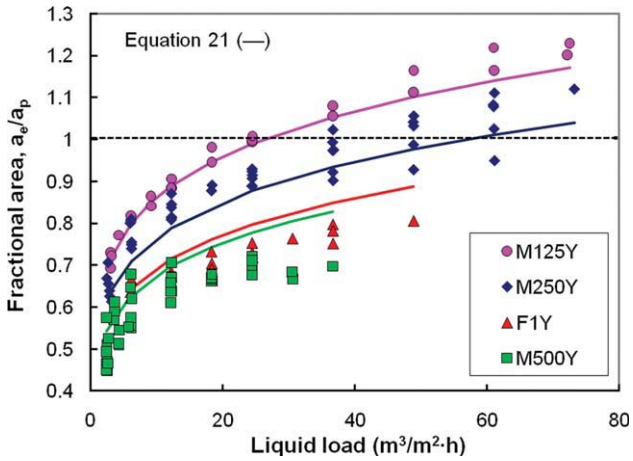

Figure 3. Mass-transfer area data for M125Y (a_p = 125 m^2/m^3), M250Y (a_p = 250 m^2/m^3), F1Y (a_p = 410 m^2/m^3), and M500Y (a_p = 500 m^2/m^3).

[Color figure can be viewed in the online issue, which is available at wileyonlinelibrary.com.]

used, but as might be expected of a structured packing, little mass transfer apparently occurred beyond the packing surface. This behavior is in contrast with random packing, where the effective area often exceeds the nominal area, sometimes by more than 50%.[40] The fact that M125Y exhibited an even higher (10%) fractional area than M250Y was striking. M125Y, being a coarser packing, would experience a greater relative impact of factors like end or wall effects. These factors were not accounted for but could be worth contemplating, since a subtraction of such effects would shift the high-end values of not only M125Y but also packings like M250Y closer to unity and, therefore, yield arguably more sensible results in the context of the expected performance limitations of structured packing. Interpreting the data at face value for this analysis, the fractional area efficiency of structured packings as they become coarser can be seen to increase and tend toward that of random packings. This trend could be related to the onset of flow instabilities (i.e., rippling or droplet formation), as Henriques de Brito et al.[41] speculated. The fractional area data of the finer packings (F1Y and M500Y) were observed to plateau far below unity. Capillary formations such as liquid bridges and menisci could be a problem for these packings due to their structural density and could explain the poorer efficiencies.

To demonstrate the ability of Eq. 21 to collapse the various data sets, the results in Figure 3 have been re-plotted in dimensionless form in Figure 4. The (Q/L_p) values are shown along the top axis to illustrate that the key to relating the data was essentially finding the appropriate combination of liquid load and geometry. The (Q/L_p) term can be considered as a generalized liquid load that is more fundamentally meaningful, although perhaps a bit more abstract, than the conventional liquid load ($m^3/m^2{\cdot}h$). The fit of the results on this basis is by no means perfect. The F1Y and M500Y data are over predicted, and the M250Y and M125Y data are under predicted. The model also fails to capture subtle aspects like the tendency of F1Y and M500Y to flatten out. Further improvements can be made. The inclusion of an additional geometric parameter could be required to

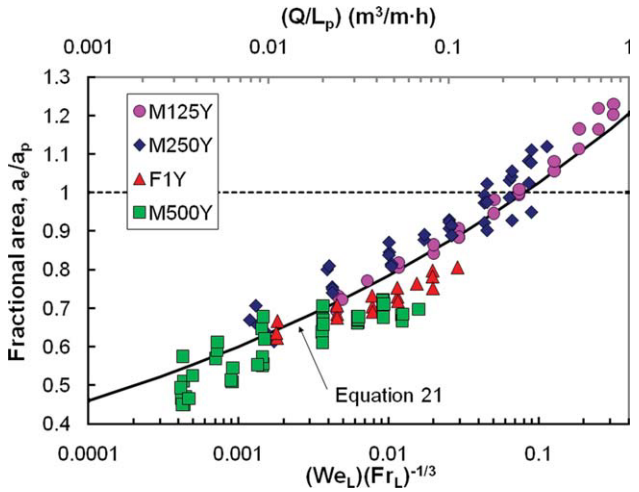

Figure 4. Representation of M125Y/M250Y/F1Y/M500Y data on dimensionless basis (bottom axis), and as a function of flow rate per wetted perimeter (top axis).

[Color figure can be viewed in the online issue, which is available at wileyonlinelibrary.com.]

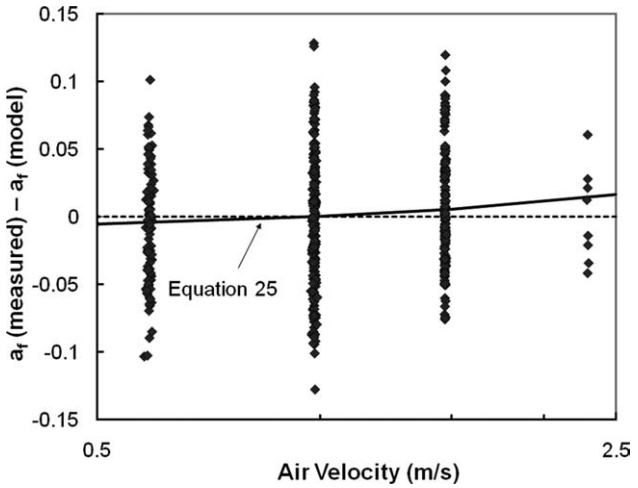

Figure 5. Residuals of mass-transfer area database as a function of air velocity, with a_f (model) values from Eq. 24.

adequately account for phenomena like liquid accumulation induced by the constricted sheets of the finer packings. Equation 24 is presented as an example, in which a dimensionless geometric term (*GD*), defined as the ratio of the column diameter to the packing channel side (*S*), has been incorporated into the original regression (Eq. 20). (A quadratic form for *GD* was found to work best while maintaining a minimal number of terms.) The constants and standard errors are provided in Eq. 24a

$$\ln a_f = C_1 \ln\left[(We_L)(Fr_L)^{-1/3}\right] + C_2[\ln(GD)]^2 + C_3 \qquad (24)$$

$$\ln a_f \pm 0.059; \quad C_1 = 0.104 \pm 0.002; \quad C_2 = -0.011 \pm 0.001; \quad C_3 = 0.363 \pm 0.011 \qquad (24a)$$

The residuals are improved with the addition of *GD* (standard error of 0.059 vs. 0.065 for Eq. 20), which could theoretically account for a number of factors, such as liquid distribution, end effects, or wall effects. Further speculation on *GD*, as well as on the importance of end and wall effects, can be found in Tsai.[16] The addition of a term like *GD* should be recognized to offer potential improvement but not be justifiable without further insight, since it was somewhat arbitrarily defined and was not validated (only a single column diameter was tested). Equation 21 is still endorsed over this modified model.

Effect of air rate

The residuals of the database as a function of air velocity are displayed in Figure 5. The predicted values from Eq. 24 (rather than Eq. 21) have been used for this purpose. Neither equation possessed terms relating to gas velocity so there was not any inherent bias in using one over the other. Equation 24 merely provided a tighter fit of the data and was used for the sake of better resolution. The simple linear fit of the residuals is given by Eq. 25, with the regressed constants shown in Eq. 25a

$$a_f(\text{measured}) - a_f(\text{model}) = C_1 u_G + C_2 \qquad (25)$$

$$[a_f(\text{measured}) - a_f(\text{model})] \pm 0.046; \quad C_1 = 0.011 \pm 0.006; \quad C_2 = -0.011 \pm 0.007 \qquad (25a)$$

The measured area in this work was concluded to be insensitive to the air rate. This conclusion is consistent with many of the structured packing models in the literature.[3] As such, it was considered acceptable to treat the data obtained at different air rates (at a given liquid load) on equivalent terms and average them for clarity, as shown with M250Y in Figure 6.

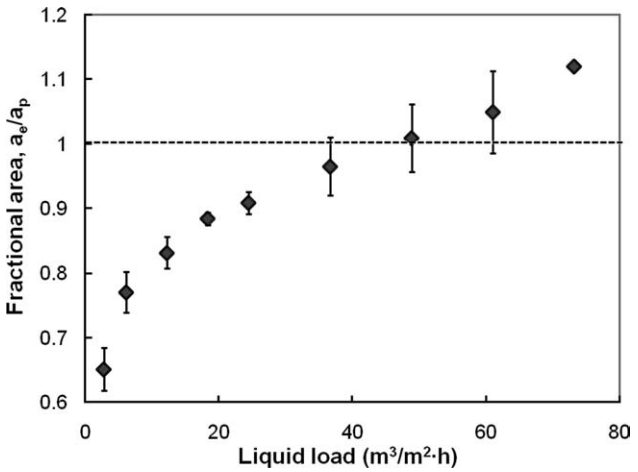

Figure 6. Averaged mass-transfer area data for M250Y (a_p = 250 m^2/m^3).

Error bars denote one standard deviation.

Effect of surface tension (M250Y/M500Y/P500)

Before presenting the surface-tension-related results, the lack of explicit mention of the solid–liquid contact angle in this work should first and foremost be discussed, since various studies have considered this to be an important parameter in the context of packing mass-transfer area.[4,42,43] Nicolaiewsky and Fair[44] performed numerous contact angle measurements on structured packing-like surfaces and found there to be good correlation of the surface tension and contact angle for a given surface. Tsai et al.[15] measured the contact angles of 0.1 kmol/m^3 NaOH solutions (either pure or with TERGITOL NP-7 added) on stainless steel and also observed a direct scaling of the contact angle with surface tension. Contact angle and surface tension were presumed to have the same meaning for the purpose of the current work. Surface tension was the more convenient parameter to relate to and reproducibly measure and, hence, report.

Extensive tests showed that the mass-transfer area was always enhanced by a reduction in surface tension (30 mN/m). The effective area was higher by 15–20% on average for the fine packings (500-series), whereas the increase was 10% or less for the coarse ones (250-series and lower). The data sets for M250Y (Figure 7) and M500Y/P500 (Figure 8) are shown for illustration. The improvement was fairly constant for every packing as a function of liquid load. This consistency suggests that the 10% enhancement was perhaps not attributable to liquid spreading or wettability, but rather some other mechanism such as creation of satellite droplets or wave formation. The additional 5–10% distinction between coarse and fine packings, which Eq. 21 is notably not able to account for, was believed to be related to capillary phenomena.

It should be recognized that Tsai et al.[15] presented mass-transfer area data for M250Y and M500Y, and concluded that a reduction in surface tension (35 mN/m) from the base case (72 mN/m) had no impact on M250Y and a dramatic effect (50%) on M500Y. Improvements to the experimental setup since then (see Tsai[16]) could explain the discrepancy between the more recent data and this previous report. The past results were not included in the current database.

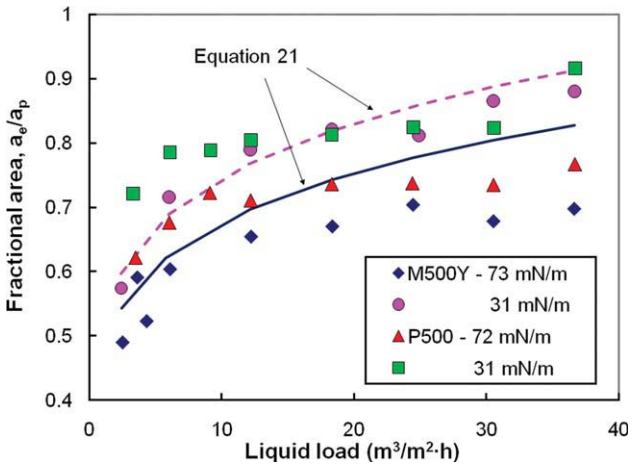

Figure 8. Averaged mass-transfer area data for M500Y and P500 (a_p = 500 m^2/m^3) for base case and at low-surface tension.

[Color figure can be viewed in the online issue, which is available at wileyonlinelibrary.com.]

Effect of liquid viscosity

The experimental design consisted of three viscosity conditions: baseline or low (ca. 1 mPa·s), intermediate (ca. 5 mPa·s), and high (ca. 10 mPa·s). Viscosity could not be increased without also changing surface tension because POLYOX WSR N750 affects both parameters (see conditions in Table 2). The residuals have been plotted as a function of viscosity in Figure 9. The intent of presenting the results in this manner, rather than displaying the raw data, was to remove the expected impact of surface tension from the analysis via its inclusion in the model values (note that

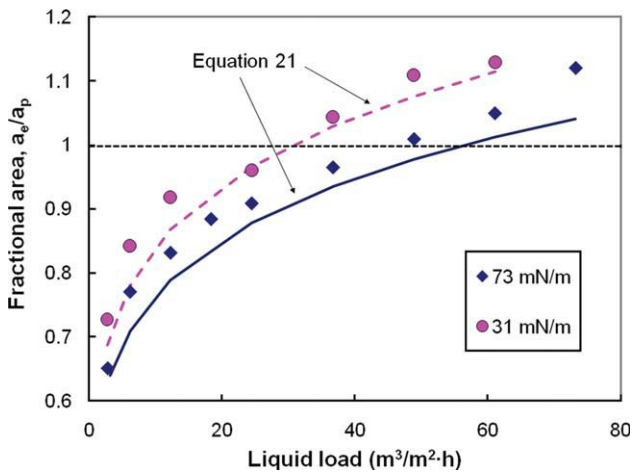

Figure 7. Averaged mass-transfer area data for M250Y (a_p = 250 m^2/m^3) for base case and at low-surface tension.

[Color figure can be viewed in the online issue, which is available at wileyonlinelibrary.com.]

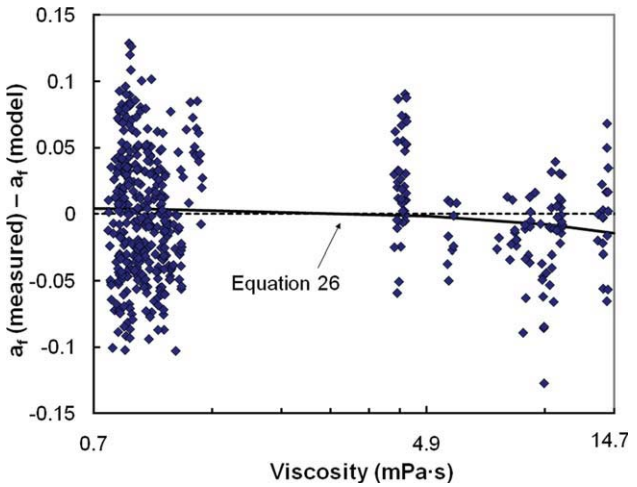

Figure 9. Residuals of mass-transfer area database as a function of liquid viscosity, with a_f (model) values from Eq. 24.

[Color figure can be viewed in the online issue, which is available at wileyonlinelibrary.com.]

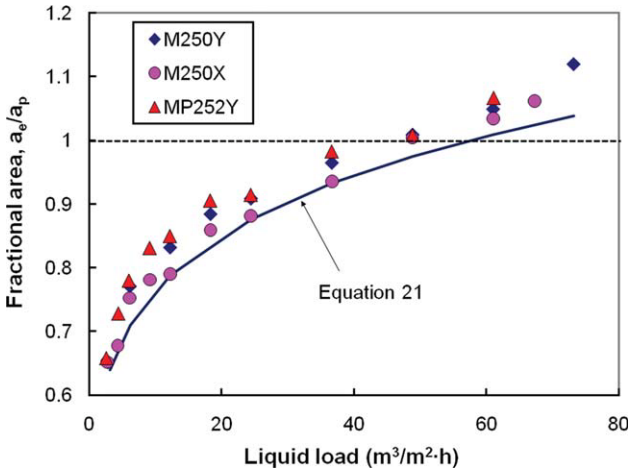

Figure 10. Averaged mass-transfer area data for M250Y, M250X, and MP252Y (a_p = 250 m^2/m^3).

[Color figure can be viewed in the online issue, which is available at wileyonlinelibrary.com.]

Eq. 21 contains a surface tension term). The line through the residuals is given by Eq. 26

$$a_f(\text{measured}) - a_f(\text{model}) = C_1 \mu_L + C_2 \tag{26}$$

$$[a_f(\text{measured}) - a_f(\text{model})] \pm 0.046;$$
$$C_1 = -0.001 \pm 0.001; \quad C_2 = 0.005 \pm 0.003 \tag{26a}$$

The statistics (Eq. 26a) were not supportive of any meaningful trend. Viscosity was concluded to have no impact on the mass-transfer area over the range of tested values.

An elevated viscosity would intuitively result in a thicker liquid film on the packing surface. In the idealized scenario of a smooth, inclined plate, this change would raise the gas-liquid contact plane but would not necessarily affect the interfacial area, in concurrence with the experimental findings. Actual flow experiments, such as those performed by Shi and Mersmann[43] and Nicolaiewsky et al.,[45] however, would suggest viscosity to influence spreading and, hence, the effective area. The viscosity limits in these studies were notably more expansive than the one in the current work (1–15 mPa·s). As such, the possibility that viscosity could become significant at higher values cannot be discounted. The tested range may not have been broad enough to appreciably affect the spreading of liquid relative to the channel dimensions.

Effect of corrugation angle (M250Y/M250X) and element interface (M250Y/MP252Y)

The M250Y, M250X, and MP252Y mass-transfer area data are shown in Figure 10. M250X had steeper flow channels (60°) than M250Y (45°), but otherwise was geometrically equivalent. Its measured area appears to be lower than M250Y but by less than 5% — insufficient to be distinguished from the experimental noise. The two packings were concluded to have the same effective area. Past investigations[46,47] have shown 45 and 60° packings to differ by 20 to 30% in terms of overall mass-transfer efficiency, but this difference could be entirely attributable to gas-side mass-transfer coefficients (and not necessarily areas).

The interface between packing elements, often referred to as the joint, is known to exhibit a higher fractional holdup than the element itself and is where flooding tends to be initiated.[34,48] High-capacity packings have been introduced to counteract this problem.[49,50] The idea is to bend the sheets near the joint from the standard 45° inclination to a vertical (90°) orientation to facilitate a smoother flow transition. The packing used in this work (MP252Y) resembled M250Y except for this modification, which occurred at the top/bottom 1.25-cm of each 21-cm tall element. The channel dimensions (*S, B, h*) matched those of M250Y, and the specific area was assumed to be 250 m^2/m^3 as well. (Alix and Raynal[35] notably listed slightly different dimensions for MP252Y than the values in Table 2, but even if their numbers were used, the calculated wetted perimeters of MP252Y and M250Y would still be within 3% of each other.) The M250Y and MP252Y data (Figure 10) were indistinguishable, which would suggest that the joint does not tangibly contribute to the mass-transfer area. The fact that the majority of data was collected far from the loading region, where one would not expect there to be a great deal of gas-liquid turbulence between elements, could explain the lack of an effect.

While M250Y, M250X, and MP252Y exhibited very similar mass-transfer areas; their pressure drop behavior was quite contrasting. Figures 11 and 12, respectively, compare the results under dry and irrigated (24.4 $m^3/m^2 \cdot h$, with water) conditions. The data have been normalized by Eq. 27, a power-law expression obtained from a regression of the M250Y dry pressure drop data as a function of the gas-flow factor (F_G)

$$\frac{\Delta P_{\text{dry,M}}250\text{Y}}{Z} = 30.92 F_G^{1.8555} \tag{27}$$

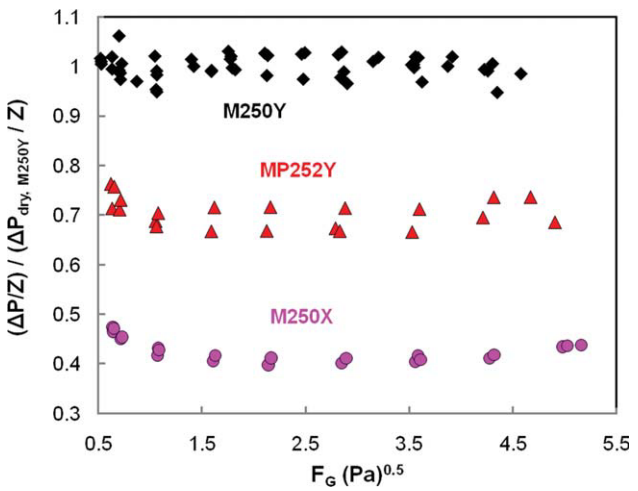

Figure 11. Normalized dry pressure-drop data for M250Y, M250X, and MP252Y.

[Color figure can be viewed in the online issue, which is available at wileyonlinelibrary.com.]

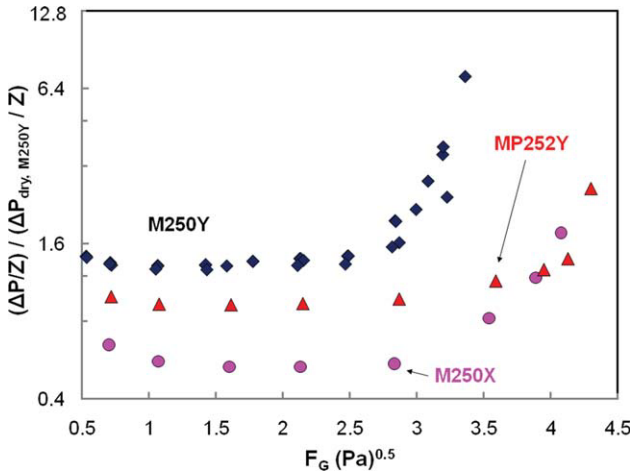

Figure 12. Normalized pressure-drop data for M250Y, M250X, and MP252Y at liquid load of 24.4 $m^3/m^2 \cdot h$.

[Color figure can be viewed in the online issue, which is available at wileyonlinelibrary.com.]

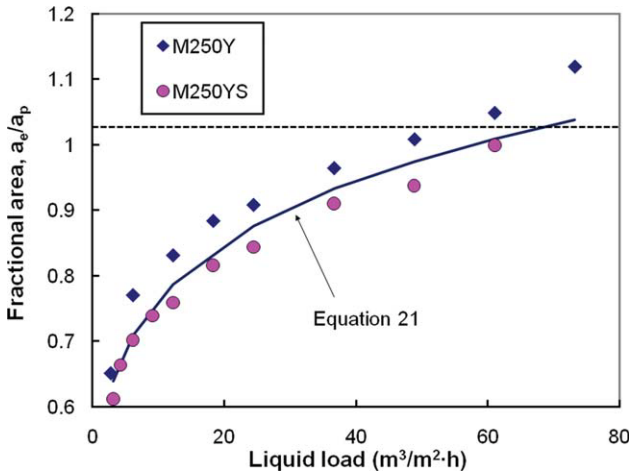

Figure 13. Averaged mass-transfer area data for M250Y and M250YS (a_p = 250 m^2/m^3).

[Color figure can be viewed in the online issue, which is available at wileyonlinelibrary.com.]

The M250X and MP252Y dry pressure drops were 40 and 70% of those of M250Y; this approximate ratio was maintained even under irrigated conditions (preloading). The channel configuration would appear to have a far greater impact on the vapor-flow path (i.e., hydraulics) than on the liquid (i.e., wetted area).

It obviously would not make sense to select M250Y over M250X or MP252Y on the criterion of effective area alone, on account of its significantly poorer hydraulic aspects. The M250X/MP252Y tradeoff is not as straightforward. The former offered a lower pressure drop, whereas the latter seemed to better resist flooding. Based on these findings, geometric designs not currently commercially available but seemingly worth pursuing might include a packing with channels steeper than 60° or a hybrid 60°/smoothed joint packing ("MellapakPlus 252X").

Effect of texture (M250Y/M250YS)

Figure 13 displays the mass-transfer area results for M250Y and M250YS. M250YS was an untextured (smooth) version of M250Y, but the two packings were otherwise geometrically identical and were both assumed to have a specific area of 250 m^2/m^3. The M250YS points appear to be consistently lower (10%) than the M250Y points, which could be because the embossing had an enhancing effect (e.g., related to turbulence), or because it simply served to increase the specific area (and actually had no mass-transfer-related benefits). Either theory could be valid, so the only definite conclusion that can be made is that texture provides a weak contribution at most to the mass-transfer area.

Comparison with literature models

Tsai et al.[29] demonstrated the models of Rocha et al.[4] and Billet and Schultes[5] to be poor in their handling of aqueous systems. For Rocha et al., at least, this poor accuracy could be partly due to a reliance on distillation data, which generally consist of very low-surface tension systems. An important objective of this research was to establish a model suitable for aqueous conditions, but ideally, this model would be universally applicable. To test this objective, Eq. 21 was evaluated at conditions reported in a distillation study (cyclohexane/*n*-heptane at 414 kPa) conducted by the SRP.[46] Figure 14 compares Eq. 21 with the literature correlations for this condition and for water for M250Y. The 20% greater area for cyclohexane/*n*-heptane was a somewhat liberal extrapolation of the 10% effect observed in the experiments conducted in the current work (30 mN/m), but at the very least, the predicted values were plausible, ranging from 0.74 to 1.18. Obviously, it is impossible to say whether or not Eq. 21 is truly correct under these circumstances, since no independent measurements of area exist for validation. Still,

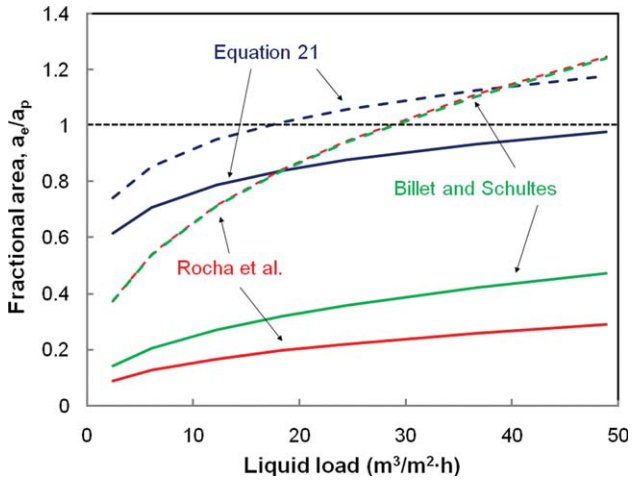

Figure 14. Predicted mass-transfer area of M250Y from various models (a_p = 250 m^2/m^3).

Lines denote water (—) (ρ_L = 1000 kg/m^3, μ_L = 1 mPa·s, σ = 72 mN/m) or cyclohexane/*n*-heptane system at 414 kPa (– –) (ρ_L = 561 kg/m^3, μ_L = 0.16 mPa·s, σ = 8 mN/m). [Color figure can be viewed in the online issue, which is available at wileyonlinelibrary.com.]

one cannot deny that the correlation offers reasonable predictions for both aqueous and hydrocarbon systems and, therefore, appears to be more flexible than Rocha et al. and Billet and Schultes, which certainly do not handle the former well. Nevertheless, because Eq. 21 was developed using aqueous systems, it remains best suited for applications of this nature. As with any model, caution should be exercised when extrapolating beyond the databank on which it was based.

The convergence of the literature models for cyclohexane/*n*-heptane is perhaps indicative of a common or similar databank basis. The better agreement with Eq. 21 (relative to the water scenario), particularly at moderate liquid loads (25–50 $m^3/m^2{\cdot}h$), is worth noting. Using these literature correlations for aqueous systems is not recommended, but they could actually be acceptable when applied toward distillation-type systems.

Conclusions

Rates of absorption of CO_2 into 0.1 $kmol/m^3$ NaOH were measured. The k'_g models for the base case, low-surface tension (125 ppm_v TERGITOL NP-7 + 50 g/m^3 Dow Corning Q2-3183A antifoam), and high viscosity (1.25 wt % POLYOX WSR N750) systems were found to match the data within 10% and were, therefore, believed to be acceptable for use with no further modifications.

The mass-transfer area of nine structured packings was measured via absorption of CO_2 into 0.1 $kmol/m^3$ NaOH. The global model that was regressed as a function of $(We_L)(Fr_L)^{-1/3}$ was capable of representing the entire database with acceptable accuracy (±13%). It was also satisfactory in its treatment of both aqueous and hydrocarbon systems, unlike the Rocha et al.[4] and Billet and Schultes[5] correlations. The model was not without flaws, although, and most notably was unable to account for two features that distinguished the high a_p packings from the others: a more prominent asymptote with liquid load and a stronger dependence on surface tension. Both were theorized to be a function of internal liquid bridging and could possibly be captured with appropriate adjustments to the correlation.

Packing size (125–500 m^2/m^3), and liquid load (2.5–75 $m^3/m^2{\cdot}h$) had the largest influence on the mass-transfer area. A greater area was usually associated with a higher liquid load, and fractional area (a_e/a_p) efficiency generally increased with increasing coarseness.

A reduction in surface tension (30 mN/m) enhanced the mass-transfer area. The difference was more pronounced for the finer packings (15–20%) than for the coarser ones (10%). No significant dependence on gas velocity (0.6–2.3 m/s) or liquid viscosity (1–15 mPa·s) was observed.

Flow channel configuration (45° vs. 60° or smoothed element interfaces) had essentially no bearing on the effective area but drastically affected the hydraulics. Dry and preloading pressure drops for the 250-series packings were in the order: M250X (0.4) < MP252Y (0.7) < M250Y, with the numbers in parentheses representing the values relative to M250Y.

The effect of surface texture on the mass-transfer area was debatable but was weak at best; the gain from embossing (vs. smooth) was a maximum of 10%.

Acknowledgments

This work was supported by the Luminant Carbon Management Program, the Process Science and Technology Center, and the Industrial Associates Program for CO_2 Capture by Aqueous Absorption. The authors thank Sulzer Chemtech (Mark Pilling) and Koch-Glitsch, Inc. (Randy Hardy) for supplying the packing materials for this research and for their technical support. The assistance of J. Christopher Lewis, Peter Schultheiss, Andreas Kettner, and the Separations Research Program staff members is gratefully acknowledged.

Notation

A = cross-sectional area of column, m^2
a_e = effective area of packing, m^2/m^3
a_f = fractional area of packing
a_p = specific (geometric) area of packing, m^2/m^3
B = packing channel base, m
C_1, C_2, C_3 = constants in Eqs. 17, 20, 24–26
$D_{CO2,L}$ = diffusion coefficient of CO_2 in solution, m^2/s
$D_{OH-,L}$ = diffusion coefficient of OH^- in solution, m^2/s
E = enhancement factor
E_∞ = enhancement factor for instantaneous, irreversible reaction
F_G = gas-flow factor ($= u_G(\rho_G)^{0.5}$), $(m/s)(kg/m^3)^{0.5}$ or $(Pa)^{0.5}$
Fr_L = Froude number for liquid
g = gravitational constant; 9.81 m/s^2
GD = geometric dimension
H_{CO2} = Henry's constant of CO_2, $m^3{\cdot}Pa/kmol$
h = packing crimp height, m
Ha = Hatta number
$HETP$ = height equivalent to a theoretical plate, m
K_G = overall mass-transfer coefficient, $kmol/m^2{\cdot}Pa{\cdot}s$
k_1 = pseudo-first-order reaction rate constant, s^{-1}
k_G = gas-side mass-transfer coefficient, $kmol/m^2{\cdot}Pa{\cdot}s$
k'_g = mass-transfer parameter, $kmol/m^2{\cdot}Pa{\cdot}s$
k^0_L = (physical) liquid-side mass-transfer coefficient, m/s
k_{OH-} = second-order reaction rate constant, $m^3/kmol{\cdot}s$
L_p = wetted perimeter in cross-sectional slice of packing, m
N_{CO2} = molar flux of CO_2, $kmol/m^2{\cdot}s$
P = pressure, Pa
P^*_{CO2} = equilibrium partial pressure of CO_2, Pa
P^i_{CO2} = partial pressure of CO_2 at gas-liquid interface, Pa
Q = volumetric flow rate, m^3/s
R = ideal gas constant, 8314.5 $m^3{\cdot}Pa/kmol{\cdot}K$
r = chemical reaction rate, $kmol/m^3{\cdot}s$
S = packing channel side, m
T = temperature, K
u_G = superficial gas velocity, m/s
$u_{L,film}$ = average liquid film velocity, m/s
We_L = Weber number for liquid
y = mole fraction in vapor phase
y^* = equilibrium mole fraction of vapor with liquid
$y_{CO2,in/out}$ = mole fraction of CO_2 at inlet/outlet
Z = packed height, m
z = location in packed bed, m

Greek letters

α = corrugation angle (with respect to the horizontal), deg
ΔP = pressure drop, Pa
δ = liquid film thickness, m
μ_L = liquid viscosity, kg/m·s or Pa·s
ρ_G = gas density, kg/m^3
ρ_L = liquid density, kg/m^3
σ = surface tension, N/m

Literature Cited

1. Aroonwilas A, Tontiwachwuthikul P, Chakma A. Effects of operating and design parameters on CO_2 absorption in columns with structured packings. *Sep Purif Technol*. 2001;24:403–411.
2. Luo S, Li H, Fei W, Wang Y-d. Liquid film characteristics on surface of structured packing. *Chin J Chem Eng*. 2009;17:47–52.

3. Wang GQ, Yuan XG, Yu KT. Review of mass-transfer correlations for packed columns. *Ind Eng Chem Res.* 2005;44:8715–8729.
4. Rocha JA, Bravo JL, Fair JR. Distillation columns containing structured packings: a comprehensive model for their performance. 2. Mass-transfer model. *Ind Eng Chem Res.* 1996;35:1660–1667.
5. Billet R, Schultes M. Predicting mass transfer in packed columns. *Chem Eng Technol.* 1993;16:1–9.
6. Hoffmann A, Maćkowiak JF, Górak A, Haas M, Löning J-M, Runowski T, Hallenberger K. Standardization of mass transfer measurements: A basis for the description of absorption processes. *Chem Eng Res Des.* 2007;85:40–49.
7. Rejl JF, Linek V, Moucha T, Valenz L. Methods standardization in the measurement of mass-transfer characteristics in packed absorption columns. *Chem Eng Res Des.* 2009;87:695–704.
8. Freeman SA, Dugas RE, Van Wagener D, Nguyen T, Rochelle GT. Carbon dioxide capture with concentrated, aqueous piperazine. *Int J Greenhouse Gas Control.* 2010;4:119–124.
9. Weiland RH, Dingman JC, Cronin DB, Browning GJ. Density and viscosity of some partially carbonated aqueous alkanolamine solutions and their blends. *J Chem Eng Data.* 1998;43:378–382.
10. Henni A, Hromek JJ, Tontiwachwuthikul P, Chakma A. Volumetric properties and viscosities for aqueous amp solutions from 25 to 70°C. *J Chem Eng Data.* 2003;48:551–556.
11. Vázquez G, Alvarez E, Navaza JM, Rendo R, Romero E. Surface tension of binary mixtures of water + monoethanolamine and water + 2-amino-2-methyl-1-propanol and tertiary mixtures of these amines with water from 25 to 50°C. *J. Chem Eng Data.* 1997;42:57–59.
12. Derks PW, Hogendoorn KJ, Versteeg GF. Solubility of N_2O in and density, viscosity, and surface tension of aqueous piperazine solutions. *J Chem Eng Data.* 2005;50:1947–1950.
13. Sharma MM, Danckwerts PV. Chemical methods of measuring interfacial area and mass transfer coefficients in two-fluid systems. *Br Chem Eng.* 1970;15:522–528.
14. Perry D, Nutter DE, Hale A. Liquid distribution for optimum packing performance. *Chem Eng Prog.* 1990;86:30–35.
15. Tsai RE, Schultheiss P, Kettner A, Lewis JC, Seibert AF, Eldridge RB, Rochelle GT. Influence of surface tension on effective packing area. *Ind Eng Chem Res.* 2008;47:1253–1260.
16. Tsai RE. Mass Transfer Area of Structured Packing. University of Texas at Austin, Austin, TX, 2010. Ph.D Dissertation.
17. Bishnoi S, Rochelle GT. Absorption of carbon dioxide into aqueous piperazine: reaction kinetics, mass transfer, and solubility. *Chem Eng Sci.* 2000;55:5531–5543.
18. Cullinane JT, Rochelle GT. Kinetics of carbon dioxide absorption into aqueous potassium carbonate and piperazine. *Ind Eng Chem Res.* 2006;45:2531–2545.
19. Bishnoi S. Carbon Dioxide Absorption and Solution Equilibrium in Piperazine Activated Methyldiethanolamine. University of Texas at Austin, Austin, TX, 2000. PhD Dissertation.
20. Danckwerts PV. *Gas-Liquid Reactions.* New York: McGraw-Hil; 1970.
21. Kucka L, Kenig EY, Gorak A. Kinetics of the gas-liquid reaction between carbon dioxide and hydroxide ions. *Ind Eng Chem Res.* 2002;41:5952–5957.
22. Haubrock J, Hogendoorn JA, Versteeg GF. The applicability of activities in kinetic expressions: A More Fundamental Approach to Represent the Kinetics of the System CO_2-OH- in terms of activities. *Int. J. Chem. React. Eng.* 2005;3:1–17.
23. Pohorecki R, Moniuk W. Kinetics of reaction between carbon dioxide and hydroxyl ions in aqueous electrolyte solutions. *Chem Eng Sci.* 1988;43:1677–1684.
24. Pigford RL. Counter-Diffusion in a Wetted Wall Column. University of Illinois at Urbana-Champaign, Urbana, IL, 1941. PhD Dissertation.
25. Hobler T. *Mass Transfer and Absorbers.* Oxford: Pergamon Press; 1966.
26. Bird RB, Stewart WE, Lightfoot EN. *Transport Phenomena.* 2nd ed. New York: John Wiley & Sons, Inc.; 2002.
27. Pacheco MA. Mass Transfer, Kinetics and Rate-based Modeling of Reactive Absorption. University of Texas at Austin, Austin, TX, 1998. PhD Dissertation.
28. Lohse M, Alper E, Quicker G, Deckwer WD. Diffusivity and solubility of carbon dioxide in diluted polymer solutions. *AIChE J.* 1981;27:626–631.
29. Tsai RE, Seibert AF, Eldridge RB, Rochelle GT. Influence of viscosity and surface tension on the effective mass transfer area of structured packing. *Energy Procedia.* 2009;1:1197–1204.
30. Olujic Z, Kamerbeek AB, de Graauw J. A corrugation geometry based model for efficiency of structured distillation packing. *Chem Eng Process.* 1999;38:683–695.
31. Sidi-Boumedine R, Raynal L. Influence of the viscosity on the liquid hold-up in trickle-bed reactors with structured packings. *Catal Today.* 2005;105:673–679.
32. Petre CF, Larachi F, Iliuta I, Grandjean BPA. Pressure drop through structured packings: Breakdown into the contributing mechanisms by CFD modeling. *Chem Eng Sci.* 2003;58:163–177.
33. Aroonwilas A. Mass-Transfer with Chemical Reaction in Structured Packing for CO_2 Absorption Process. University of Regina, Regina, Saskatchewan; 2001. PhD Dissertation.
34. Suess P, Spiegel L. Hold-up of mellapak structured packings. *Chem Eng Process.* 1992;31:119–124.
35. Alix P, Raynal L. Liquid distribution and liquid hold-up in modern high capacity packings. *Chem Eng Res Des.* 2008;86:585–591.
36. Spiegel L, Meier W. Correlations of the performance characteristics of the various Mellapak types. *ICHEME Symp Ser.* 1988;104:A203–A215.
37. Moniuk W, Pohorecki R. Viscosity and density of sodium and potassium alkaline solutions. *Hung J Ind Chem.* 1991;19:175–178.
38. Haar L, Gallagher JS, Kell GS. *NBS/NRC Steam Tables: Thermodynamic and Transport Properties and Computer Programs for Vapor and Liquid States of Water in SI Units.* Washington, DC: Hemisphere Publishing Corp; 1984.
39. Rocha JA, Bravo JL, Fair JR. Distillation columns containing structured packings: a comprehensive model for their performance. 1. Hydraulic models. *Ind Eng Chem Res.* 1993;32:641–651.
40. Wilson I. Gas-Liquid Contact Area of Random and Structured Packing. University of Texas at Austin, Austin, TX; 2004. MS. Thesis.
41. Henriques de Brito M, von Stockar U, Bangerter AM, Bomio P, Laso M. Effective mass-transfer area in a pilot plant column equipped with structured packings and with ceramic rings. *Ind Eng Chem Res.* 1994;33:647–656.
42. McGlamery GG. Liquid Film Transport Characteristics of Textured Metal Surfaces. University of Texas at Austin, Austin, TX, 1988. PhD Dissertation.
43. Shi MG, Mersmann A. Effective interfacial area in packed columns. *Ger Chem Eng.* 1985;8:87–96.
44. Nicolaiewsky EMA, Fair JR. Liquid flow over textured surfaces. 1. Contact angles. *Ind Eng Chem Res.* 1999;38:284–291.
45. Nicolaiewsky EMA, Tavares FW, Rajagopal K, Fair JR. Liquid film flow and area generation in structured packed columns. *Powder Technol.* 1999;104:84–94.
46. Olujic Z, Seibert AF, Fair JR. Influence of corrugation geometry on the performance of structured packings: an experimental study. *Chem Eng Process.* 2000;39:335–342.
47. Fair JR, Seibert AF, Behrens M, Saraber PP, Olujic Z. Structured packing performance - experimental evaluation of two predictive models. *Ind Eng Chem Res.* 2000;39:1788–1796.
48. Green CW, Farone J, Briley JK, Eldridge RB, Ketcham RA, Nightingale B. Novel application of X-ray computed tomography: determination of gas/liquid contact area and liquid holdup in structured packing. *Ind Eng Chem Res.* 2007;46:5734–5753.
49. Moser F, Kessler A. Increased capacity thanks to improved geometry. *Sulzer Tech. Rev.* 1999;81:24–26.
50. Olujic Z, Jansen H, Kaibel B, Rietfort T, Zich E. Stretching the capacity of structured packings. *Ind Eng Chem Res.* 2001;40:6172–6180.

Manuscript received Apr. 7, 2010, and revision received June 11, 2010.